Search for nucleon decay via modes favored by supersymmetric grand unification models in Super-Kamiokande-I

K.Kobayashi,[1] M.Earl,[2, *] Y.Ashie,[3] J.Hosaka,[3] K.Ishihara,[3] Y.Itow,[3] J.Kameda,[3] Y.Koshio,[3] A.Minamino,[3] C.Mitsuda,[3] M.Miura,[3] S.Moriyama,[3] M.Nakahata,[3] T.Namba,[3] R.Nambu,[3] Y.Obayashi,[3] M.Shiozawa,[3] Y.Suzuki,[3] Y.Takeuchi,[3] K.Taki,[3] S.Yamada,[3] M.Ishitsuka,[4] T.Kajita,[4] K.Kaneyuki,[4] S.Nakayama,[4] A.Okada,[4] K.Okumura,[4] T.Ooyabu,[4] C.Saji,[4] Y.Takenaga,[4] S.Desai,[2] E.Kearns,[2] S.Likhoded,[2] J.L.Stone,[2] L.R.Sulak,[2] W.Wang,[2] M.Goldhaber,[5] D.Casper,[6] J.P.Cravens,[6] W.Gajewski,[6] W.R.Kropp,[6] D.W.Liu,[6] S.Mine,[6] M.B.Smy,[6] H.W.Sobel,[6] C.W.Sterner,[6] M.R.Vagins,[6] K.S.Ganezer,[7] J.E.Hill,[7] W.E.Keig,[7] J.S.Jang,[8] J.Y.Kim,[8] I.T.Lim,[8] K.Scholberg,[9] C.W.Walter,[9] R.W.Ellsworth,[10] S.Tasaka,[11] G.Guillian,[12] A.Kibayashi,[12] J.G.Learned,[12] S.Matsuno,[12] D.Takemori,[12] M.D.Messier,[13] Y.Hayato,[14] A.K.Ichikawa,[14] T.Ishida,[14] T.Ishii,[14] T.Iwashita,[14] T.Kobayashi,[14] T.Maruyama,[14, †] K.Nakamura,[14] K.Nitta,[14] Y.Oyama,[14] M.Sakuda,[14, ‡] Y.Totsuka,[14] A.T.Suzuki,[15] M.Hasegawa,[16] K.Hayashi,[16] I.Kato,[16] H.Maesaka,[16] T.Morita,[16] T.Nakadaira,[16] T.Nakaya,[16] K.Nishikawa,[16] T.Sasaki,[16] S.Ueda,[16] S.Yamamoto,[16] M.Yokoyama,[16] T.J.Haines,[17, 6] S.Dazeley,[18] S.Hatakeyama,[18] R.Svoboda,[18] E.Blaufuss,[19] J.A.Goodman,[19] G.W.Sullivan,[19] D.Turcan,[19] A.Habig,[20] Y.Fukuda,[21] C.K.Jung,[1] T.Kato,[1] M.Malek,[1] C.Mauger,[1] C.McGrew,[1] A.Sarrat,[1] E.Sharkey,[1] C.Yanagisawa,[1] T.Toshito,[22] K.Miyano,[23] N.Tamura,[23] J.Ishii,[24] Y.Kuno,[24] M.Yoshida,[24] S.B.Kim,[25] J.Yoo,[25] H.Okazawa,[26] T.Ishizuka,[27] Y.Choi,[28] H.K.Seo,[28] Y.Gando,[29] T.Hasegawa,[29] K.Inoue,[29] J.Shirai,[29] A.Suzuki,[29] M.Koshiba,[30] Y.Nakajima,[31] K.Nishijima,[31] T.Harada,[32] H.Ishino,[32] Y.Watanabe,[32] D.Kielczewska,[33, 6] J.Zalipska,[33] H.G.Berns,[34] R.Gran,[34] K.K.Shiraishi,[34] A.Stachyra,[34] K.Washburn,[34] and R.J.Wilkes[34]

(The Super-Kamiokande Collaboration)

[1]*Department of Physics and Astronomy, State University of New York, Stony Brook, NY 11794-3800, USA*
[2]*Department of Physics, Boston University, Boston, MA 02215, USA*
[3]*Kamioka Observatory, Institute for Cosmic Ray Research, University of Tokyo, Kamioka, Gifu, 506-1205, Japan*
[4]*Research Center for Cosmic Neutrinos, Institute for Cosmic Ray Research, University of Tokyo, Kashiwa, Chiba 277-8582, Japan*
[5]*Physics Department, Brookhaven National Laboratory, Upton, NY 11973, USA*
[6]*Department of Physics and Astronomy, University of California, Irvine, Irvine, CA 92697-4575, USA*
[7]*Department of Physics, California State University, Dominguez Hills, Carson, CA 90747, USA*
[8]*Department of Physics, Chonnam National University, Kwangju 500-757, Korea*
[9]*Department of Physics, Duke University, Durham, NC 27708 USA*
[10]*Department of Physics, George Mason University, Fairfax, VA 22030, USA*
[11]*Department of Physics, Gifu University, Gifu, Gifu 501-1193, Japan*
[12]*Department of Physics and Astronomy, University of Hawaii, Honolulu, HI 96822, USA*
[13]*Department of Physics, Indiana University, Bloomington, IN 47405-7105, USA*
[14]*High Energy Accelerator Research Organization (KEK), Tsukuba, Ibaraki 305-0801, Japan*
[15]*Department of Physics, Kobe University, Kobe, Hyogo 657-8501, Japan*
[16]*Department of Physics, Kyoto University, Kyoto 606-8502, Japan*
[17]*Physics Division, P-23, Los Alamos National Laboratory, Los Alamos, NM 87544, USA*
[18]*Department of Physics and Astronomy, Louisiana State University, Baton Rouge, LA 70803, USA*
[19]*Department of Physics, University of Maryland, College Park, MD 20742, USA*
[20]*Department of Physics, University of Minnesota, Duluth, MN 55812-2496, USA*
[21]*Department of Physics, Miyagi University of Education, Sendai,Miyagi 980-0845, Japan*
[22]*Department of Physics, Nagoya University, Nagoya, Aichi 464-8602, Japan*
[23]*Department of Physics, Niigata University, Niigata, Niigata 950-2181, Japan*
[24]*Department of Physics, Osaka University, Toyonaka, Osaka 560-0043, Japan*
[25]*Department of Physics, Seoul National University, Seoul 151-742, Korea*
[26]*International and Cultural Studies, Shizuoka Seika College, Yaizu, Shizuoka 425-8611, Japan*
[27]*Department of Systems Engineering, Shizuoka University, Hamamatsu, Shizuoka 432-8561, Japan*
[28]*Department of Physics, Sungkyunkwan University, Suwon 440-746, Korea*
[29]*Research Center for Neutrino Science, Tohoku University, Sendai, Miyagi 980-8578, Japan*
[30]*University of Tokyo, Tokyo 113-0033, Japan*
[31]*Department of Physics, Tokai University, Hiratsuka, Kanagawa 259-1292, Japan*
[32]*Department of Physics, Tokyo Institute for Technology, Meguro, Tokyo 152-8551, Japan*
[33]*Institute of Experimental Physics, Warsaw University, 00-681 Warsaw, Poland*
[34]*Department of Physics, University of Washington, Seattle, WA 98195-1560, USA*
(Dated: February 7, 2008)

We report the results for nucleon decay searches via modes favored by supersymmetric grand unified models in Super-Kamiokande. Using 1489 days of full Super-Kamiokande-I data, we searched

arXiv:hep-ex/0502026v1 15 Feb 2005

for $p \rightarrow \bar{\nu}K^+$, $n \rightarrow \bar{\nu}K^0$, $p \rightarrow \mu^+K^0$ and $p \rightarrow e^+K^0$ modes. We found no evidence for nucleon decay in any of these modes. We set lower limits of partial nucleon lifetime 2.3×10^{33}, 1.3×10^{32}, 1.3×10^{33} and 1.0×10^{33} years at 90% confidence level for $p \rightarrow \bar{\nu}K^+$, $n \rightarrow \bar{\nu}K^0$, $p \rightarrow \mu^+K^0$ and $p \rightarrow e^+K^0$ modes, respectively. These results give a strong constraint on supersymmetric grand unification models.

PACS numbers: Valid PACS appear here

I. INTRODUCTION

Grand Unified Theories (GUTs) [1, 2] seek to unify the strong and electroweak forces. They are motivated by the apparent merging of the coupling constants of the strong, weak, and electromagnetic forces at a large energy scale ($\sim 10^{16}$ GeV) when low energy measurements are extrapolated. One of the generic predictions of GUTs is the instability of the proton, as well as neutrons bound inside the nucleus. The experimental observation of nucleon decay would provide a strong evidence of GUTs.

In GUTs, nucleon decay can proceed via an exchange of a massive boson between two quarks in a proton or in a bound neutron. In this reaction, one quark transforms into a lepton and another into an anti-quark which binds with a spectator quark creating a meson. The favored decay mode in the prototypical GUT [2] based on an $SU(5)$ symmetry ("minimal $SU(5)$") is $p \rightarrow e^+\pi^0$. For this decay, the proton lifetime scales as $\sim M_X^4$, where M_X is the mass of the heavy vector gauge boson. In minimal $SU(5)$, M_X is on the order of the coupling unification at 10^{15} GeV/c^2, yielding a predicted proton lifetime of $\tau/B(p \rightarrow e^+\pi^0) \sim 10^{29\pm2}$ years. The first generation large water Cherenkov detector experiments [3, 4], motivated by this prediction, observed no evidence of proton decay in this mode and ruled out the model. Also, the recent result by the Super-Kamiokande experiment extended the previous results [5]. It turns out that this contradiction of $SU(5)$ with the experimental proton decay limit can be resolved by incorporating supersymmetry (SUSY) in the theories.

Supersymmetry postulates that, for every SM particle, there is a corresponding "superpartner" with spin differing by 1/2 unit from the SM particle [6]. The additional particles stabilize the renormalization of the Higgs boson and address the so-called "hierarchy problem". When one incorporates the superpartners into the calculation of the running of the coupling constants, the convergence of the coupling constants occurs at an unification scale about one order of magnitude larger than that of minimal $SU(5)$. Since the proton decay rate via $p \rightarrow e^+\pi^0$ scales as M_X^{-4}, this leads to a suppression of about four orders

of magnitude in the rate, consistent with experimental non-observation of $p \rightarrow e^+\pi^0$. Furthermore, while in the minimal $SU(5)$ model, the three coupling constants do not quite meet at a single point within three standard deviations, they meet together at a single point in the minimal SUSY $SU(5)$ model [7].

However, in many SUSY GUT models, other dominant nucleon decay modes occur via dimension five operator interactions with the exchange of a heavy supersymmetric color triplet Higgsino [8]. These interactions suppress transitions from one quark family in the initial state to the same family in the final state. Since the only second or third generation quark which is kinematically allowed is the strange quark, an anti-strange quark typically appears in the final state for these interactions. The anti-strange quark binds with a spectator quark to form a K meson in the final state. Thus, SUSY GUTs favor nucleon decays in $p \rightarrow \bar{\nu}K^+$ and $n \rightarrow \bar{\nu}K^0$ modes. The predictions for the nucleon lifetime in SUSY GUT models, however, varies widely, and may even be suppressed, since there are many new free parameters introduced because of the supersymmetry breaking.

In the minimal SUSY $SU(5)$ GUTs, the partial proton lifetime is estimated to be $\tau/B(p \rightarrow \bar{\nu}K^+) \leq 2.9 \times 10^{30}$ years [9]. Other models have been proposed beyond those based on $SU(5)$. In particular, models based on $SO(10)$ symmetry have become popular in light evidence for neutrino mass [10], which they naturally accommodate. An important property of the $SO(10)$ symmetry is that there is a heavy right-handed neutrino in a multiplet containing the matter fields. In addition, all matter fields of one generation can be contained in a single multiplet, in contrast to theories based on $SU(5)$ where they must be broken into two separate representations.

One class of models [11], predicts the partial proton lifetime for $p \rightarrow \bar{\nu}K^+$ mode to be less than 10^{34} years, which is within the observable range of Super-Kamiokande. In addition, the same mechanism which gives mass to the neutrinos provides a new set of dimension five operators through which the proton can decay. A consequence of this is that the prediction for $p \rightarrow \mu^+K^0$ decay rate is within a factor of 10 of the $p \rightarrow \bar{\nu}K^+$ decay rate.

These decay modes, favored by SUSY GUT models, have been searched for in water Cherenkov detector [3, 4, 29] and iron calorimeter [12, 13] experiments. The best limits on the partial nucleon lifetime via $p \rightarrow \bar{\nu}K^+$, $n \rightarrow \bar{\nu}K^0$, $p \rightarrow \mu^+K^0$, and $p \rightarrow e^+K^0$ are 6.7×10^{32} years [29], 8.6×10^{31} years [4], 1.2×10^{31} years [3, 4, 13], and 1.5×10^{31} years [4], respectively.

*Present address: University of Maryland School of Medicine, Baltimore, MD 21201, USA

†Present address: Department of Physics, Univ. of Tsukuba, Tsukuba, Ibaraki 305 8577, Japan

‡Present address: Department of Physics, Okayama University, Okayama 700-8530, Japan

II. SUPER-KAMIOKANDE DETECTOR

The Super-Kamiokande detector [14] is a 50 kton water Cherenkov detector located at the Kamioka Observatory of Institute for Cosmic Ray Research in the Kamioka mine. It lies 1,000 m underneath the top of Mt. Ikenoyama, (i.e. 2,700 m water equivalent underground), resulting in a cosmic ray muon rate of 2.2 Hz, a reduction of 10^{-5} compared to the rate at the surface. The detector is optically separated into two regions, the inner and outer detectors (ID and OD). The ID of the Super-Kamiokande-I detector, which operated from April 1996 to July 2001, was instrumented with 11,146 50-cm diameter inward facing photomultiplier tubes (PMTs) which provide 40% photocathode coverage. This photocathode coverage makes it possible to detect low energy electrons down to ~5 MeV. The ID volume is the sensitive region for nucleon decay searches and has a total fiducial volume of 22.5 kton, defined as a cylindrical volume with surfaces 2 m away from the ID PMT plane. The OD completely surrounds the ID and is instrumented with 1,885 20-cm diameter outward facing PMTs equipped with 60 cm × 60 cm wavelength shifter plates to increase light collection efficiency. The main purpose of the OD is to tag incoming cosmic ray muons and exiting muons induced by atmospheric neutrinos. A detailed description of the Super-Kamiokande-I detector can be found elsewhere [14].

III. DATA SET

Data used for this analysis is taken during the period from May 1996 to July 2001. It corresponds to 1489 days of data taking and an exposure of 92 kt·year.

IV. NUCLEON DECAY EVENT AND BACKGROUND SIMULATION

In order to search for nucleon decay in the Super-Kamiokande detector, it is critical to understand the signal event signature and background characteristics. We simulate specific decay modes of nucleon decay as well as background events using a signal event generator and the standard Super-Kamiokande atmospheric Monte Carlo (MC). By comparing the characteristics of these signal and background simulated events in detail, we establish the optimum event selection criteria. When we limit the nucleon decay events to occur only in the Super-Kamiokande fiducial volume, the only significant background to nucleon decays originate from atmospheric neutrino interactions. Once the selection criteria are established, the detection efficiency is then estimated by analyzing the nucleon decay MC sample, and the expected background is estimated by analyzing the atmospheric neutrino MC sample.

A. Nucleon decay event simulation

Nucleon decay in water can occur from a free proton in the hydrogen nucleus or from a bound nucleon in the oxygen nucleus. It is relatively simple to simulate the free proton decay using the Super-Kamiokande MC. However, simulation of the bound nucleon decays requires special care, because of various nuclear effects experienced by the daughter particles from nucleon decay before they exit the nucleus.

Nucleons bound in oxygen have Fermi momentum and nuclear binding energy. In our simulation, we use the Fermi momentum distribution measured by an electron-^{12}C scattering experiment [15]. For nucleon decays in an oxygen nucleus, the nucleon mass must be modified by nuclear binding energy. The modified nucleon mass m'_N is calculated by $m'_N = m_N - E_{bind}$ where m_N is the nucleon rest mass and E_{bind} is the nuclear binding energy. Yamazaki and Akaishi [16] estimated the effective nucleon mass when the nucleon decays in ^{16}O. Ten percent of decays are from a nucleus which has wave functions correlated with other nucleons in the nucleus. Figure 1 shows the invariant proton mass distribution in ^{16}O used in the $p \rightarrow \bar{\nu}K^+$ MC simulation. The correlated decays produce the broad nucleon mass distribution below around 850 MeV/c^2.
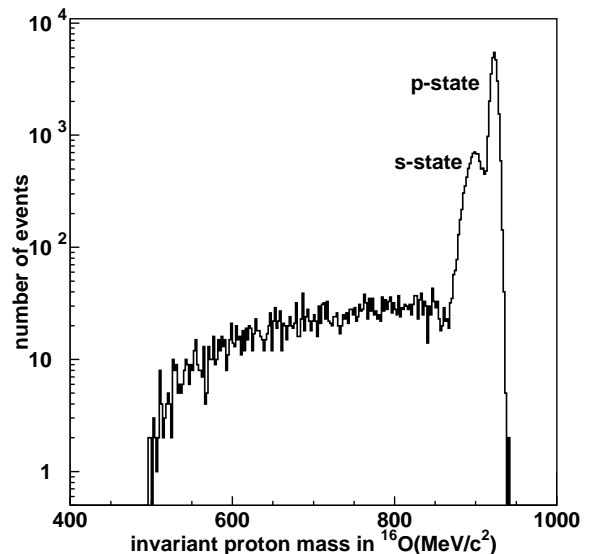

FIG. 1: The invariant proton mass distribution in ^{16}O in the $p \rightarrow \bar{\nu}K^+$ MC simulation [16]. The distributions of s- and p-states are expressed by Gaussian function $G(mean, RMS)$. It is $G(938.3 - 39.0, 10.2))$ MeV/c^2 for s-state and $G(938.3 - 15.5, 3.82))$ MeV/c^2 for p-state.

When a nucleon decays in the oxygen nucleus, the remaining nucleus can be in an excited state and it can emit prompt gamma-rays during its subsequent de-excitation process. This process was studied by Ejiri [17] and we use his results in this analysis. This prompt gamma-ray provides us with a powerful tool to tag $p \rightarrow \bar{\nu}K^+$ events.

The decay products of a nucleon bound in oxygen can interact hadronically with the remaining protons and neutrons in the residual ^{15}N nucleus before exiting. The initial position of the nucleon is assumed to have the Woods-Saxon density distribution [18]:

$$\rho(r) = \frac{\rho(0)}{1 + \exp\left(\frac{r-a}{b}\right)}, \qquad (1)$$

where a (=1.07 A$^{1/3}$ = 2.69 fm for ^{16}O) is the average of nuclear radius, $2b$ (=0.82 fm) is the thickness of the nuclear surface, and r is the distance from the center of the nucleus. Interactions relevant to this analysis are K^+N and K^0N elastic scatterings, and K^+N and K^0N inelastic scatterings via charge exchange. The K^+p reactions can proceed elastically or inelastically. Inelastic interactions are due to the $K^+p \rightarrow K^+\Delta$. A partial wave analysis for the scattering amplitudes was performed by Hyslop et al. [19] by doing a global fit to many data samples. The maximum momentum for the kaon from the nucleon decays is about 600 MeV/c. Below 800 MeV/c, K^+p scattering has an extremely small contribution from inelastic scattering. Therefore a K^+ from a proton decay via $p \rightarrow \bar{\nu}K^+$ effectively experiences only elastic scatterings with protons in the residual nucleus. Since $p \rightarrow \bar{\nu}K^+$ are identified through the detection of the daughter particles of the kaon decay at rest, K^+p scattering does not affect the detection efficiency of $p \rightarrow \bar{\nu}K^+$. The charge exchange reaction $K^+n \rightarrow K^0p$ can reduce the efficiency for detecting $p \rightarrow \bar{\nu}K^+$ events. It is important to estimate what fraction of K^+ is lost due to this effect. The reaction was measured for low momentum kaons (250 to 600 MeV/c) by Glasser et al [20] yielding cross sections ranging from 2.0 $\pm$ 0.18 mb at K^+ momentum of 250 MeV/c to 6.4 $\pm$0.56 mb at K^+ momentum of 590 MeV/c. To estimate the fraction of K^+ lost due to this effect, a MC simulation is performed. K^+ are started at random points in the nucleus according to the Woods-Saxon density distribution (Equation 1). If there is an interaction, Pauli blocking is taken into account by requiring the momentum of the recoil nucleon to be above the Fermi surface momentum (p_F).

$$p_{recoil} > p_F(r) = \hbar\left(\frac{3\pi^2}{2}\rho(r)\right), \qquad (2)$$

where $\rho(r)$ is the same as defined in Equation 1. From this simulation, it is estimated that 1% of K^+ from $p \rightarrow \bar{\nu}K^+$ decays in total are lost because of this charge exchange reaction. From isospin symmetry, the K^0N reactions have essentially the same magnitude as the K^+N reactions.

We simulate propagation of the produced particles and Cherenkov light in water by custom code based on GEANT [21]. The propagation of charged pions in water is simulated by custom code based on [22] for less than 500 MeV/c and by CALOR [24] for more than 500 MeV/c.

In the $n \rightarrow \bar{\nu}K^0$, $p \rightarrow \mu^+K^0$ and $p \rightarrow e^+K^0$ searches, only decays to K_S^0 are studied because the lifetime of the K_L^0 is so long and many of them interact in water before decaying. The effect of K^0 regeneration is small in K_S^0 decay searches.

In total, 50,000 MC events are generated for each decay mode to find the signature of nucleon decays and to estimate detection efficiencies. Of these, 34,664, 34,561, 34,648 and 34,572 events are in the fiducial volume in the $p \rightarrow \bar{\nu}K^+$, $n \rightarrow \bar{\nu}K^0$, $p \rightarrow \mu^+K^0$ and $p \rightarrow e^+K^0$ MCs, respectively.

B. Atmospheric neutrino background

The most significant background to nucleon decay comes from the atmospheric neutrino interactions in the detector. Atmospheric neutrinos are produced in collisions of cosmic rays with air molecules in the atmosphere of the earth. Primary cosmic rays, mostly protons, interact hadronically with air molecules creating $\pi^{\pm}$, $K^{\pm}$, K^0, and other mesons. Neutrinos are then produced from the chain decay of these mesons. The production of atmospheric neutrinos has been calculated in great detail by many authors. For this analysis, we use the calculation by Honda et al [25].

Because the cross section for neutrinos to interact with matter is extremely small, they can travel unscattered through the earth and interact with a nucleon in the water of Super-Kamiokande via the weak interaction. A generic interaction is

$$\nu_l + N \rightarrow l + N' + X, \qquad (3)$$

where N and N' are the initial and final state nucleons, l is the outgoing lepton associated with ν_l, and X can be other possible hadronic particles such as pions. Because some of these interactions result in topologies similar to those of nucleon decays, they present a challenging background to nucleon decay searches.

We use the same atmospheric neutrino MC simulation [26] that is used for Super-Kamiokande neutrino oscillation studies with slight modifications. The modifications made for this analysis are as following: for single pion production, the so-called axial vector mass which appears in the neutrino-nucleon differential cross section is set to be 1.2 GeV/c^2 to estimate conservatively. For deep inelastic scattering, we use a model motivated by Bodek and Yang [27].

In order to estimate the atmospheric neutrino background events for the nucleon decays involving kaons, the production of kaons through the baryon resonances is included based on the model of Rein and Sehgal [28]. The cross section for kaon production is one or more than one order of magnitude smaller than that of single pion production. In addition, many charged kaons produced in neutrino interactions emit Cherenkov light while kaons from proton decay do not, and K production is accompanied by a Λ baryon which decays into either $p\pi^-$ or $n\pi^0$

in most cases. Therefore these background events can be distinguished from nucleon decay events, and their contributions to the background can be safely ignored.

In order to estimate the backgrounds from the atmospheric neutrinos to nucleon decays at a high precision, we use a total of 100 year equivalent sample of atmospheric neutrino MC simulation events for this analysis.

V. EVENT SELECTION AND RECONSTRUCTION

We apply the first stage reduction for the data to remove major background. Then we reconstruct physical quantities for data and also signal and background MC events. Data reduction and event reconstruction is the same as for the neutrino oscillation analysis [26].

A. Event Selection

The trigger threshold for events used in this analysis is set to 29 PMT hits corresponding to an electron equivalent energy of 5.7 MeV. The trigger rate at this threshold is about 10 Hz. The majority of the collected data are the events originating from cosmic muons and radioactivities. An event selection process is applied to remove these events. Almost all cosmic muons are rejected requiring no significant OD activities. After applying event reconstruction, events are rejected when their electron equivalence energy is less than 30 MeV corresponding to 197 MeV/c for muons or when the event vertex is located outside of the fiducial volume. The remaining event rate after this first stage reduction is about eight events/day. Almost all of these events originate from atmospheric neutrino interaction.

B. Event Reconstruction

Physical quantities are reconstructed for the events remaining from the event selection process. In the reconstruction, certain quantities are determined such as the event vertex, the number of visible Cherenkov rings, the direction of each ring, particle identification, momentum and number of Michel electrons. The vertex resolution is 34 cm for electrons and 25 cm for muons in single ring events. In the $p \to \bar{\nu}K^+$, $K^+ \to \mu^+\nu_\mu$ and $K^+ \to \pi^+\pi^0$ MC, the vertex resolution is 47 and 37 cm, respectively. In the $n \to \bar{\nu}K^0$, $p \to \mu^+K^0$ and $p \to e^+K^0$ MC, better resolutions are obtained. Each ring is identified as e-like ($e^\pm$,γ) or μ-like ($\mu^\pm$,$\pi^\pm$,proton) based on a likelihood analysis of Cherenkov ring pattern and Cherenkov angle. In a single ring electron or muon event, the misidentification probability is 0.5%. Momentum is determined by the sum of photo electrons (PEs) after correcting for light attenuation in water, PMT angular acceptance, PMT coverage, and the assigned electron, muon,

or pion particle assumption. The momentum of a pion is determined by Cherenkov angle as well as the sum of PEs. The momentum resolution for a 236 MeV/c muon from $p \to \bar{\nu}K^+$,$K^+ \to \mu^+\nu_\mu$ is 3% and mass resolution for π^0 from $p \to \bar{\nu}K^+$,$K^+ \to \pi^+\pi^0$ is 9%. Figure 2 shows the reconstructed π^0 invariant mass distribution in the $p \to \bar{\nu}K^+$,$K^+ \to \pi^+\pi^0$ MC. The detection efficiency of Michel electrons is estimated to be 80% for μ^+ and 63% for μ^-.
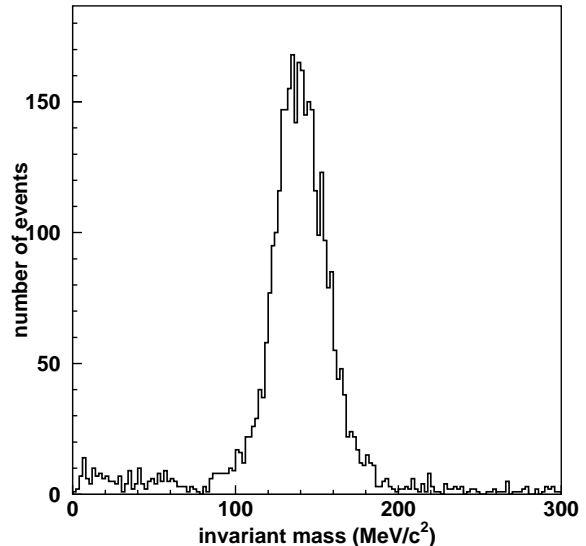

FIG. 2: The reconstructed π^0 invariant mass distribution in the $p \to \bar{\nu}K^+$,$K^+ \to \pi^+\pi^0$ MC after applying selection criteria (B1,B2) (See Section VI A).

C. Calibration

An important aspect of nucleon decay analyses is the choice of selection criteria. These criteria are dependent upon the energies of the particles produced in the various interactions. For this reason, the energy deposition and detector response of particles traversing the detector must be accurately modeled in the MC simulation. Energy scale calibrations are performed by comparing the data and MC sample of Michel electrons from stopping cosmic ray muons, π^0s produced in atmospheric neutrino interactions and stopping cosmic ray muons. The Cherenkov angle and the range are used to obtain muon momentum for stopping muons. These samples provide energy calibration varying from several tens MeV (Michel electrons) to several GeV (stopping cosmic ray muons), entirely covering the energy range relevant to nucleon decay searches. Based on these samples, the energy scale is reproduced in the MC within 2.5%.

VI. ANALYSIS

During 1,489 days of livetime corresponding to 92 kton·year of exposure, 12,179 events are recorded after the first stage reduction process. Of these, 8,207 are identified as single ring.

It has been well known for some time that there is a deficit of events induced by atmospheric muon neutrino oscillations [10]. In order to estimate accurately the actual number of background events, the atmospheric neutrino flux is normalized based on the observed deficit of μ-like events due to well established neutrino oscillation phenomena and the observed number of e-like events. The normalizing factor is determined as multiplying 0.67 for charged current ν_μ events and 1.07 for charged current ν_e and all neutral current events. Finally we normalize the 100 year MC sample (2,246 kton·years) to the 92 kton·year sample of Super-Kamiokande exposure. Based on these simulated signal and background events, we determine selection criteria for each nucleon decay mode, which is discussed in the following sections. All detection efficiencies given below include all relevant branching ratios.

A. Search for $p \to \bar{\nu} K^+$

This is the primary mode of proton decay in SUSY GUT models. A search for $p \to \bar{\nu} K^+$ was described in our previous paper [29] based on the 45 kton·year data. In that paper, we described three methods to search for this mode using the two dominant decay modes of the kaon, $K^+ \to \pi^+\pi^0$ (Method 1) and $K^+ \to \mu^+\nu_\mu$. For $K^+ \to \mu^+\nu_\mu$, we looked for both the prompt gamma-ray from the de-excitation of the residual excited ^{15}N nucleus (Method 2: prompt gamma-ray search) and for an excess in the momentum distribution of μ-like events at $p_\mu = 236$ MeV/c (Method 3: mono-energetic muon search). In this paper, we present proton lifetime limits derived using these methods including improved analyses which increase the detection efficiency and reduce the background.

1. Method 1: $K^+ \to \pi^+\pi^0$ search

If a proton decays to $\bar{\nu}$ K$^+$, the K$^+$ has low enough momentum that the majority stop before decaying. Therefore, when the K$^+$ decays to a π^+ and a π^0, these two particles go back-to-back and the π^0 momentum is expected to be mono-energetic at 205 MeV/c. To detect this type of events, the following criteria are required: (A1) two e-like rings, (A2) one Michel electron, (A3) 175 MeV/c < p_{π^0} < 250 MeV/c, (A4) 85 MeV/c^2 < m_{π^0} < 185 MeV/c^2, (A5) 40 PE < Q_{π^+} < 100 PE, (A6) Q_{res} < 70 PE. The reconstructed total momentum and invariant mass consistent with the π^0 from the two e-like rings are defined as p_{π^0} and m_{π^0}, respectively.

The π^+ momentum is so close to the Cherenkov threshold that the Cherenkov ring is not detected in most cases. However, since many backgrounds survive criteria (A1-A4), we use the Cherenkov light produced by the π^+ in addition. Q_{π^+} is sum of PEs corrected or light attenuation and PMT acceptance, which is observed in the PMTs within 40° half opening angle opposite to the π^0 direction. Q_{res} is sum of PEs in the remaining PMTs after rejecting the area within the 90° half opening angle toward the two gamma-ray directions and the Q_{π^+} searched area. We use the criterion (A6) for background rejection. The total detection efficiency for this method is estimated to be 6.0% and the background is estimated to be 0.6 events. Figure 3 shows the distribution of the Q_{π^+} versus p_{π^0} for data, the atmospheric neutrino MC and $p \to \bar{\nu} K^+$ MC. The main sources of background are events by single pion production and deep inelastic scattering. The incoming neutrino energy of the background is typically between 0.6 GeV and 2 GeV. In the data, no events pass the selection criteria (A1-A6).

2. Method 2: $K^+ \to \mu^+\nu_\mu$, prompt gamma-ray search

When a proton decays in one of the inner shells of the ^{16}O nucleus, the residual ^{15}N nucleus is left in an excited state. This state quickly de-excites with a certain probability of emitting gamma-rays. The most probable residual state is a $p_{3/2}$ 6.3 MeV state which leads to an emission of single 6.3 MeV gamma-ray [17]. Since the K$^+$ is below the Cherenkov threshold and the K$^+$ lifetime is 12.4 ns, we can separate the de-excitation gamma-ray from the μ^+ signal. The μ^+ momentum is mono-energetic (236 MeV/c), because the K$^+$ decays at rest. By requiring a prompt gamma-ray signal as well as the mono-energetic muon and an electron from the muon decay, most backgrounds are eliminated.

In order to search for the prompt gamma-ray, three quantities must be defined. The first is t_μ which is a reference time associated with the detection of the muon. The second is t_0 which is the time to begin a backward search in time of flight (TOF) subtracted timing distribution for the earlier hits from the prompt gamma-ray. Finally, t_γ is the time associated with the detection of the gamma-ray. The reference point t_μ corresponding to the muon is found by searching for the point in time when $\Delta N_{hit}/\Delta t$ is maximum where N_{hit} is number of PMT hits. The starting time t_0 is defined as the first point less than t_μ where $dN_{hit}/dt = 0$. In the t_γ search, PMTs which are within a cone with a 50° half opening angle with respect to the muon are removed. Removing these tubes enables the search for the prompt gamma-ray to start at a closer time to t_μ. A 12 ns timing window is slid backward starting with its trailing edge at t_0. The values t_γ and $N_{hit\gamma}$ are determined by maximizing the number of hits in the 12 ns sliding window. $N_{hit\gamma}$ is the maximum number of hits at t_γ in the 12 ns sliding window.
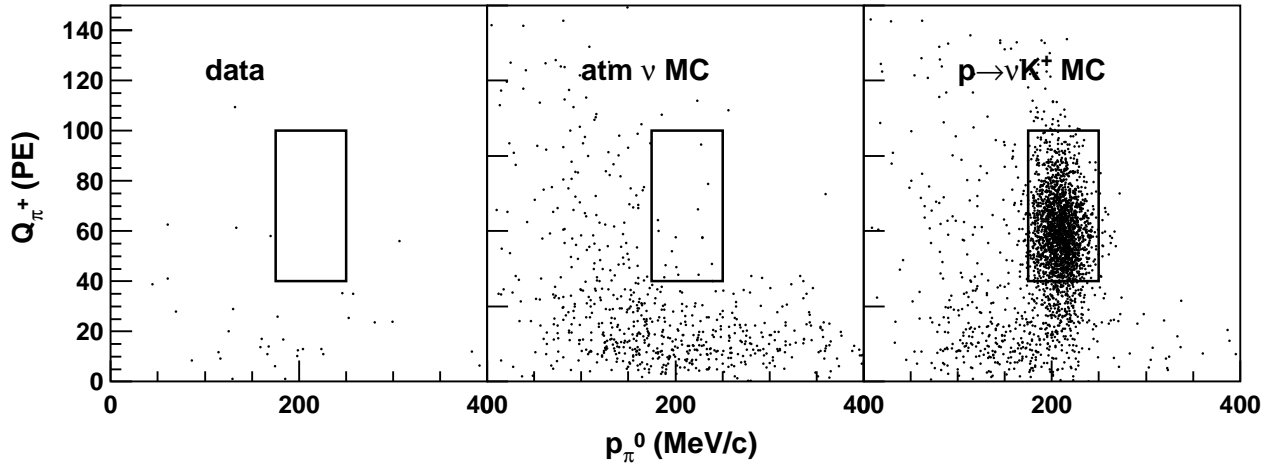
FIG. 3: The distributions of the Q_{π^+} versus p_{π^0} for events that satisfy criteria (A1,A2,A4,A6). Each figure shows: (left) data, (middle) atmospheric neutrino MC and (right) $p \to \bar{\nu}K^+$ MC. The box shows criteria (A3,A5).

Using these quantities, the following selection criteria are applied: (B1) one μ-like ring, (B2) one Michel electron, (B3) 215 MeV/$c < p_\mu < 260$ MeV/c, (B4) proton rejection, (B5) $t_\mu - t_\gamma < 100$ ns, (B6) $7 < N_{hit\gamma} < 60$. Criterion (B4) is applied for rejecting backgrounds caused by poor vertex reconstruction. Most of this type of backgrounds is recoil protons produced by neutral current interactions. Since the particle type is assumed as a muon in the vertex fit, the reconstructed vertex position of a proton is not accurate. Therefore a fake peak, which mimics gamma-rays, is sometimes produced in the TOF subtracted timing distribution. In order to reject these events, two cuts, $g \geq 0.6$ and $d_{\mu e} < 200$ cm, are applied, where g is a goodness of the TOF subtracted timing distribution and $d_{\mu e}$ is the distance between the Michel positron vertex and the muon stopping point. In proton decay events, $d_{\mu e}$ should be close to zero.

Passing the $p \to \bar{\nu}K^+$ and 100 year atmospheric neutrino MC events through criteria (B1-B6), the detection efficiency and background are estimated to be 8.6% and 0.7 events, respectively. The efficiency includes all branching ratios. Figure 4 shows $N_{hit\gamma}$ distribution for the 100 year sample of atmospheric neutrino MC normalized by livetime and neutrino oscillation, $p \to \bar{\nu}K^+$ MC, and 92 kton·yr sample of data. No events survive these selection criteria.

3. Method 3: $K^+ \to \mu^+\nu_\mu$, mono-energetic muon search

We search for a 236 MeV/c mono-energetic muon using events which are not selected in Method 2. To tag the muon, criteria (B1,B2) are applied, which are defined as in Method 2. Moreover, to obtain an independent event sample from Method 2, we apply criterion (B7) $N_{hit\gamma} \leq 7$. Figure 5 shows the muon momentum distribution of data compared with best fitted atmospheric neutrino MC. No significant excess is observed in the sig-
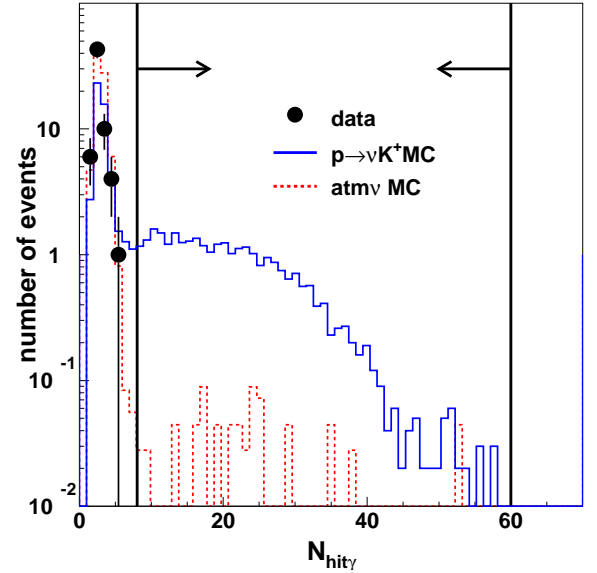

FIG. 4: The $N_{hit\gamma}$ distributions for events that satisfy criteria (B1-B5). The full circles show data and the dashed line shows atmospheric neutrino MC normalized by livetime and neutrino oscillation. The solid line shows $p \to \bar{\nu}K^+$ MC. The arrows show criterion (B6), where proton decay candidates with a prompt gamma-ray are expected.

nal region (B3). In this region, there are 181 events with a best fitted background of 200 events.

B. Search for $n \to \bar{\nu}K^0$

Many SUSY models also predict the nucleon decay mode, $n \to \bar{\nu}K^0$. We search for $n \to \bar{\nu}K^0$ using the $K_S^0 \to \pi^0\pi^0$ and $K_S^0 \to \pi^+\pi^-$ decay chain.

For the $K_S^0 \to \pi^0\pi^0$ search, the following criteria are applied: (C1) three or four e-like rings, (C2) zero Michel
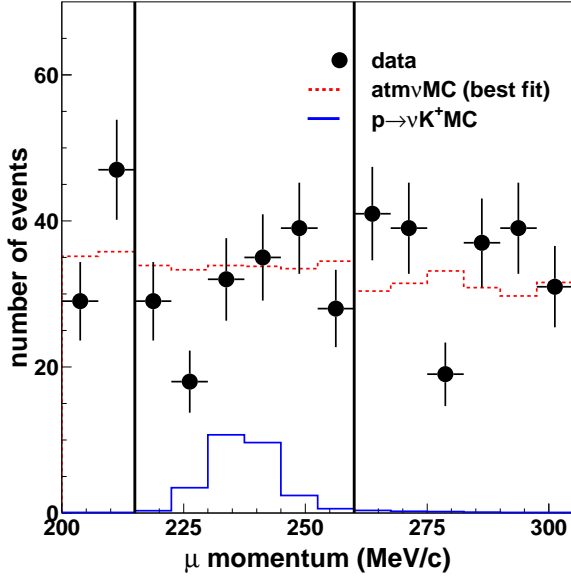
FIG. 5: The comparison between data and fitting results of muon momentum distribution for events that satisfy criteria (B1,B2,B7). The full circles show data with statistical errors. The solid line shows $p \to \bar{\nu}K^+$ MC. The dashed line shows the best fitted atmospheric neutrino MC with free normalization.

electrons, (C3) 200 MeV/c < p_{K^0} < 500 MeV/c, (C4) 400 MeV/c^2 < m_{K^0} < 600 MeV/c^2, where p_{K^0} and m_{K^0} are total momentum and invariant mass, assuming the decay sequence of K^0. Because it is difficult to identify four showering Cherenkov rings, many background events remain. About half of the background events come from deep inelastic scattering. Figure 6 shows p_{K^0} versus m_{K^0} distributions after applying criteria (C1,C2). The criteria select 14 events in the data with an expected background of 19 and a selection efficiency of 6.9%.

For the $K_S^0 \to \pi^+\pi^-$ search, the following criteria are applied: (D1) two μ-like rings, (D2) zero or one Michel electron, (D3) 200 MeV/c < p_{K^0} < 500 MeV/c, (D4) 450 MeV/c^2 < m_{K^0} < 550 MeV/c^2. Since a large fraction of π^+ or π^- momenta are below the Cherenkov threshold, the efficiency of finding both rings is low. Figure 7 shows p_{K^0} versus m_{K^0} distributions after applying criteria (D1,D2). Twenty events are observed in the data with the detection efficiency of 5.5%, while 11.2 background events are expected. Most of the background events are produced by charged current single pion production.

C. Search for $p \to \mu^+ K^0$

In a SUSY $SO(10)$ model [11] with neutrino mass, $p \to \mu^+ K^0$ is an important decay mode. We search for $p \to \mu^+ K^0$ using $K_S^0 \to \pi^0\pi^0$ and $K_S^0 \to \pi^+\pi^-$ decay chain. In this mode, the total invariant proton mass and momentum can be reconstructed and the backgrounds can be significantly reduced.

For the $K_S^0 \to \pi^0\pi^0$ search, the following criteria are

applied: (E1) 2-4 e-like rings and one μ-like ring, (E2) zero or one Michel electron, (E3) 400 MeV/c^2 < m_{K^0} < 600 MeV/c^2, (E4) 150 MeV/c < p_μ < 400 MeV/c, (E5) p_p < 300 MeV/c, (E6) 750 MeV/c^2 < m_p < 1000 MeV/c^2, where m_p and p_p are the invariant mass and total momentum assuming the decay sequence of proton, respectively. The momentum of the μ^+, p_μ, is determined using the μ-like ring. Figure 8 shows p_p versus m_p distributions after applying criteria (E1-E4). No events survive in the data with the estimated 5.4% detection efficiency and 0.4 events of the expected background.

For the $K_S^0 \to \pi^+\pi^-$ search, two different methods are applied, because ring finding efficiency of the two pions are low. The first method (Method 1) uses the following criteria: (F1) two μ-like rings, (F2) two Michel electrons, (F3) 250 MeV/c < p_μ < 400 MeV/c, (F4) p_p < 300 MeV/c. We assume the more energetic ring as muon and the other as charged pion. Figure 9 shows p_p versus p_μ distributions after applying criteria (F1,F2). The detection efficiency and the expected background are 7.0% and 3.2 events, respectively; 3 events are observed in the data. The second method (Method 2) requires: (G1) three rings, (G2) one or two Michel electrons, (G3) 450 MeV/c^2 < m_{K^0} < 550 MeV/c^2, (G4) p_p < 300 MeV/c, (G5) 750 MeV/c^2 < m_p < 1000 MeV/c^2. Figure 10 shows the p_p versus m_p distributions after applying criteria (G1-G3). The detection efficiency and the expected background are estimated to be 2.8% and 0.3 events, respectively. Most of the background events come from charged current ν_μ single pion production. No surviving events are observed in the data.

D. Search for $p \to e^+ K^0$

One of the supersymmetric theories, based on flavor group $(S_3)^3$ predicts that $p \to e^+ K^0$ occurs at a comparable rate with $p \to \bar{\nu}K^+$ and $n \to \bar{\nu}K^0$ [30]. For the search for $p \to e^+ K^0$ mode, three methods are applied in the same way as $p \to \mu^+ K^0$ search. For the $K_S^0 \to \pi^0\pi^0$ search, the selection criteria are: (H1) 3-5 e-like rings, (H2) zero Michel electrons, (H3) p_p < 300 MeV/c, (H4) 750 MeV/c^2 < m_p < 1000 MeV/c^2. We assume the most energetic ring as electron and others as gamma-rays from the π^0 decays. Figure 11 shows p_p versus m_p distributions after applying criteria (H1,H2). The detection efficiency and the expected background are 9.2% and 1.1 events, respectively. One candidate event is observed in the data.

For the $K_S^0 \to \pi^+\pi^-$ search, two different methods are applied. The first method (Method 1) uses the following criteria: (I1) one μ-like ring and one e-like ring, (I2) one Michel electron, (I3) 250 MeV/c < p_e < 400 MeV/c, (I4) p_p < 300 MeV/c, where p_e is the electron momentum determined using the e-like ring. Figure 12 shows p_p versus p_e distributions after applying criteria (I1,I2). The detection efficiency and the expected background are 7.9% and 3.6 events, respectively. Most of the background
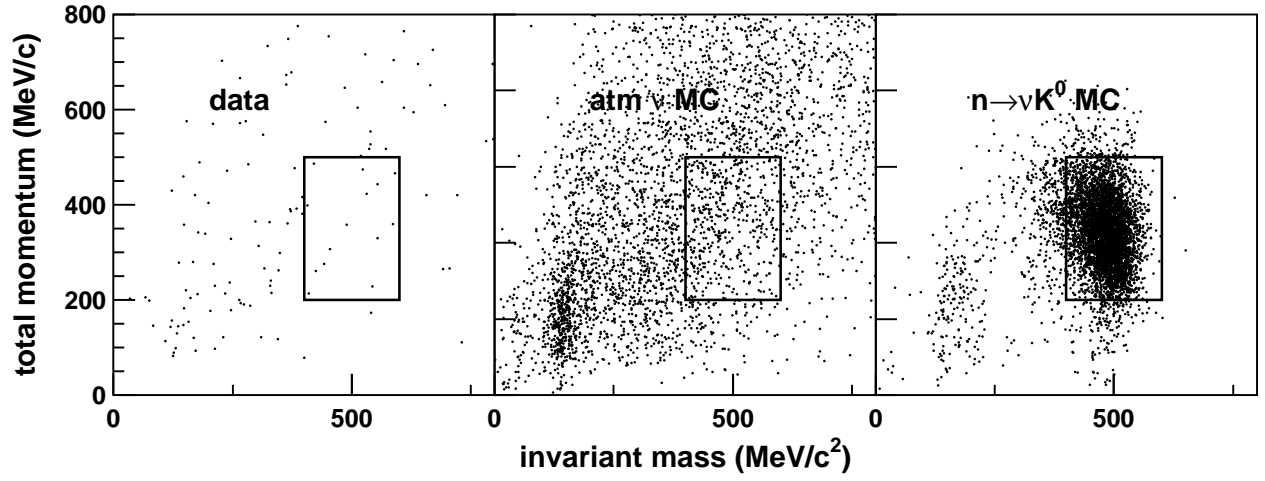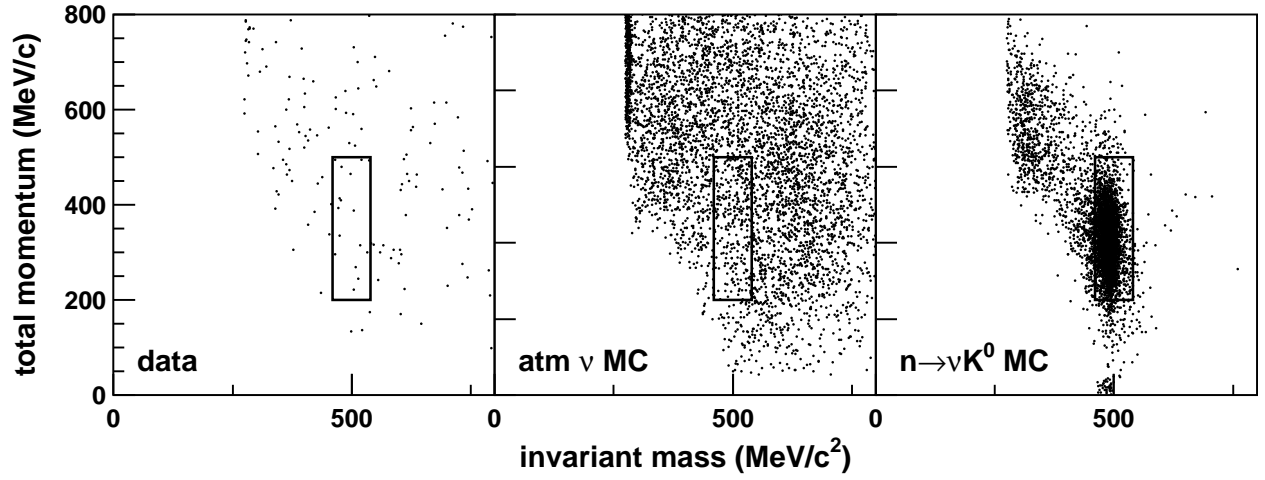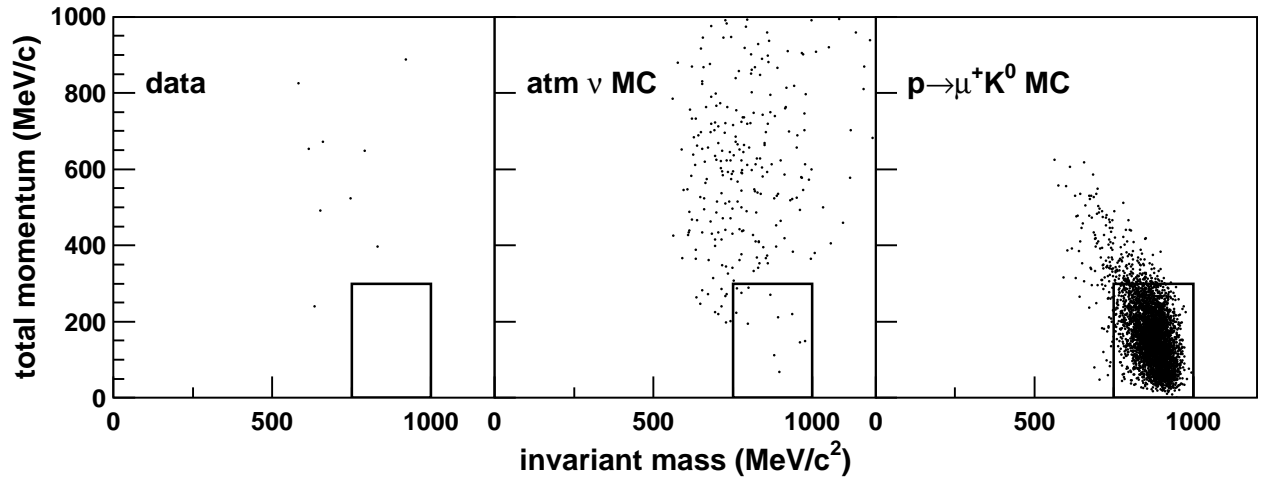
FIG. 6: The distributions of the total momentum versus invariant mass for events that satisfy criteria (C1,C2). Each figure shows: (left) data, (middle) atmospheric neutrino MC and (right) $n \to \bar{\nu}K^0$ MC. The box shows criteria (C3,C4).

FIG. 7: The distributions of the total momentum versus invariant mass for events that satisfy criteria (D1,D2). Each figure shows: (left) data, (middle) atmospheric neutrino MC and (right) $n \to \bar{\nu}K^0$ MC. The box shows criteria (D3,D4). The cluster in the atmospheric neutrino MC figure comes from mis-reconstruction.

FIG. 8: The distributions of the total momentum versus invariant mass for events that satisfy criteria (E1-E4). Each figure shows: (left) data, (middle) atmospheric neutrino MC and (right) $p \to \mu^+ K^0$ MC. The box shows criteria (E5,E6).

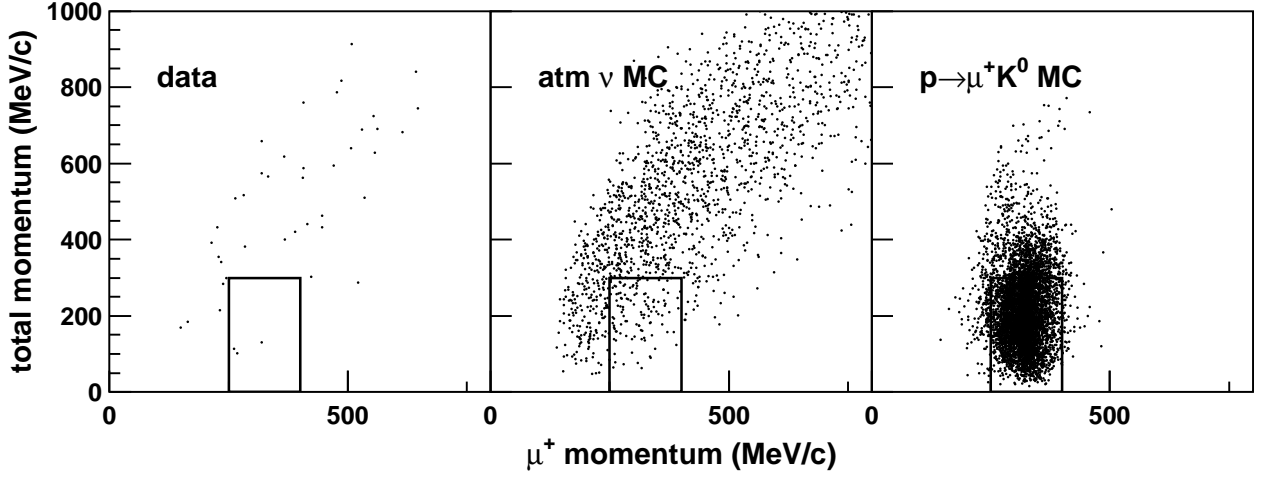FIG. 9: The distributions of the total momentum versus μ^+ momentum for events that satisfy criteria (F1,F2). Each figure shows: (left) data, (middle) atmospheric neutrino MC and (right) $p \to \mu^+ K^0$ MC. The box shows criteria (F3,F4).
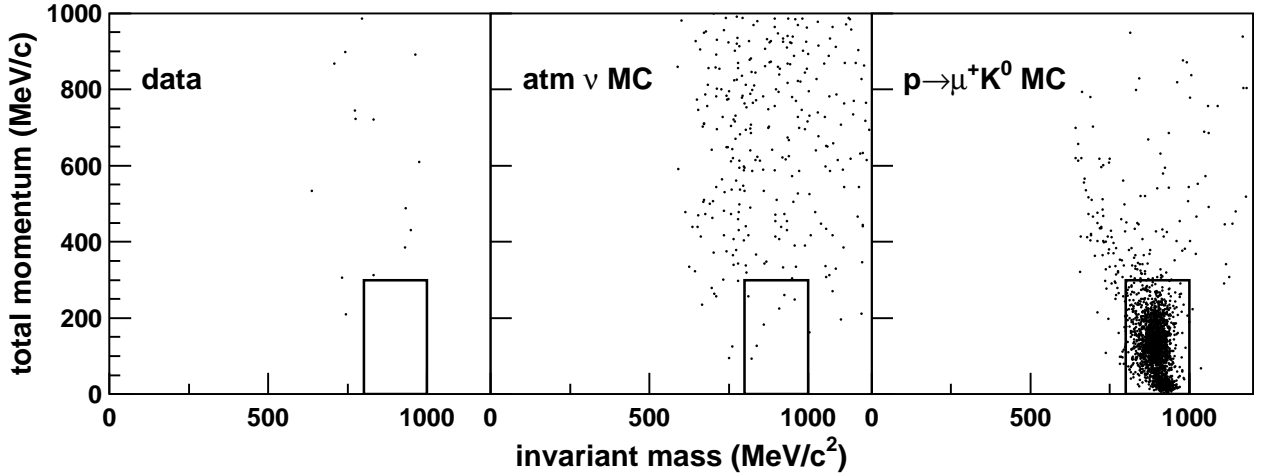

FIG. 10: The distributions of the total momentum versus invariant mass for events that satisfy criteria (G1-G3). Each figure shows: (left) data, (middle) atmospheric neutrino MC and (right) $p \to \mu^+ K^0$ MC. The box shows criteria (G4,G5).

events are produced by charged current ν_e single pion events. Five events are observed in the data. The second method (Method 2) uses the criteria: (J1) three rings (at least one e-like), (J2) zero or one Michel electron, (J3) 450 MeV/$c^2 < m_{K^0} < 550$ MeV/c^2, (J4) $p_p < 300$ MeV/c, (J5) 750 MeV/$c^2 < m_p < 1000$ MeV/c^2. Figure 13 shows p_p versus m_p distributions after applying criteria (J1-J3). The detection efficiency is estimated to be 1.3% with 0.04 expected backgrounds. No surviving events are observed in the data.

E. Systematic uncertainties

In the detection efficiency, we consider the following common systematic uncertainties in every search: imperfect knowledge of light scattering in water, energy scale, and particle identification. The uncertainty of the rate of light scattering in water is estimated to be 20%, which mainly effects on the ring finding efficiency. The energy scale uncertainty is estimated to be 2.5% by the calibration described in Section V C. For the modes which have a charged pion from kaon decay, we consider the imperfect knowledge of a charged pion-nucleon cross section in water which is estimated to be 10% by comparing with our MC and experimental data [23]. For the $p \to \mu^+ K^0$ and $p \to e^+ K^0$ search, we consider the uncertainty of the Fermi momentum which is estimated to be about 5% from model differences [15]. In addition, we consider the uncertainty of de-excitation gamma-ray emission probabilities in the $p \to \bar{\nu} K^+$, prompt gamma-ray search. It is estimated to be 15% for 6.3 MeV gamma-ray and 30% for other gamma-rays [17]. From these sources of systematic uncertainty, the total contribution to the uncertainty of the detection efficiency in the $p \to \bar{\nu} K^+$, prompt gamma-ray search is estimated to be 20%. The main
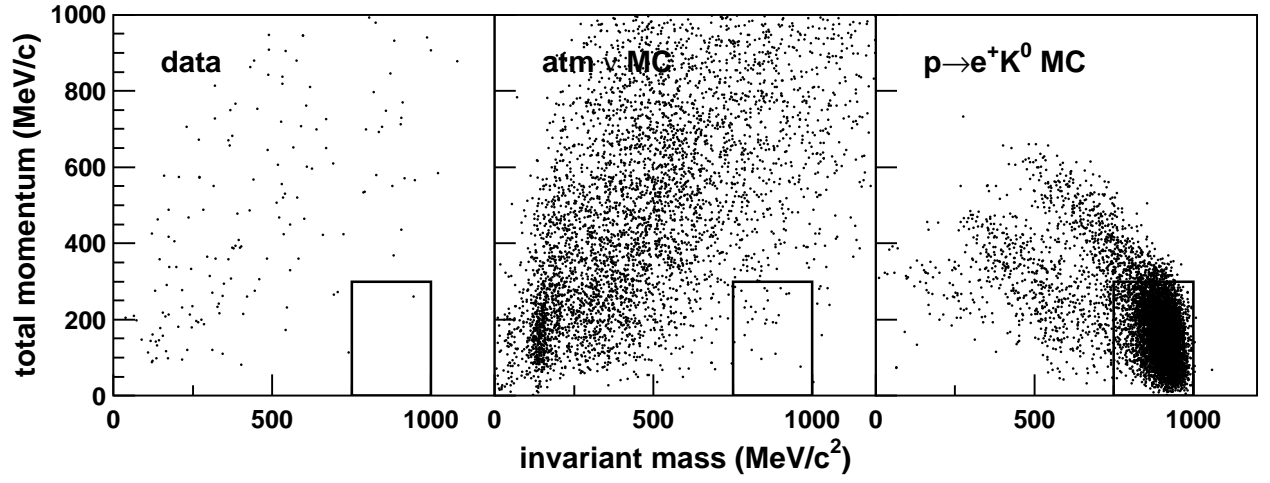
FIG. 11: The distributions of the total momentum versus invariant mass for events that satisfy criteria (H1,H2). Each figure shows: (left) data, (middle) atmospheric neutrino MC and (right) $p \rightarrow e^+ K^0$ MC. The box shows criteria (H3,H4).
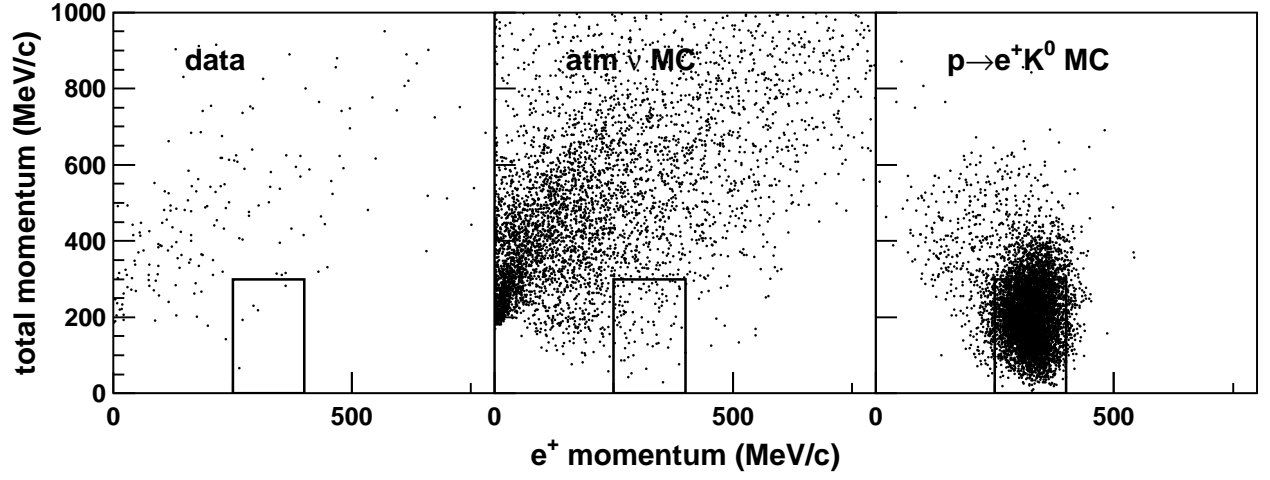

FIG. 12: The distributions of the total momentum versus e^+ momentum for events that satisfy criteria (I1,I2). Each figure shows: (left) data, (middle) atmospheric neutrino MC and (right) $p \rightarrow e^+ K^0$ MC. The box shows criteria (I3,I4).
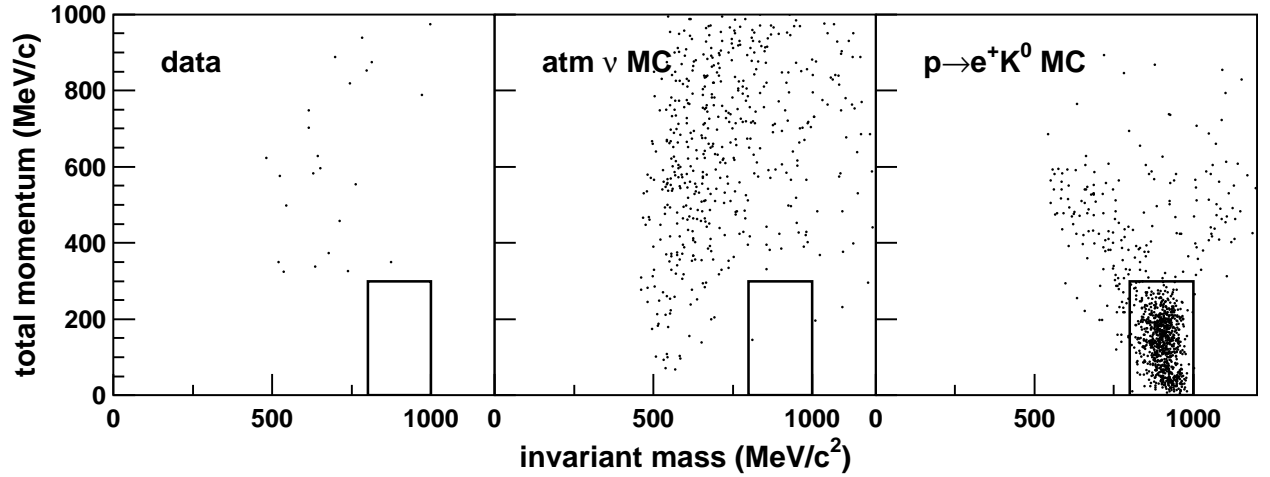

FIG. 13: The distributions of the total momentum versus invariant mass for events that satisfy criteria (J1-J3). Each figure shows: (left) data, (middle) atmospheric neutrino MC and (right) $p \rightarrow e^+ K^0$ MC. The box shows criteria (J4,J5).

uncertainty comes from the uncertainty of de-excitation gamma-ray emission probabilities. The total contributions in the $p \to \bar{\nu}K^+$, mono-energetic and $K^+ \to \pi^+\pi^0$ search are estimated to be 2.5% and 8.8%, respectively. Most of the uncertainties in the $K^+ \to \pi^+\pi^0$ search come from the imperfect knowledge of charged pion-nucleon cross section in water and light scattering in water, which are estimated to be 4.8% and 6.7%, respectively. In the $n \to \bar{\nu}K^0$ search, the total contributions are estimated to be 16% and 14% for the $K_S^0 \to \pi^0\pi^0$ and $K_S^0 \to \pi^+\pi^-$ search, respectively. The main source of uncertainty comes from the uncertainty in light scattering in water. In all methods of the $p \to \mu^+K^0$ and $p \to e^+K^0$ searches, the total contributions are less than 20%.

In the background estimation, we consider the following common systematic uncertainties in all searches: imperfect knowledge of atmospheric neutrino flux, neutrino cross sections, energy scale, and particle identification. Because we use the scaled MC, the absolute normalization error becomes smaller. However, the background uncertainty from the atmospheric neutrino flux normalization is conservatively estimated to be 20% [25]. The

imperfect knowledge of the cross sections are considered to be 30% for quasi-elastic and elastic scattering, 30% for single meson production and 50% for deep inelastic scattering. From these sources of systematic uncertainty, the total contributions to the uncertainty of the background in the $n \to \bar{\nu}K^0$, $K_S^0 \to \pi^0\pi^0$ and $K_S^0 \to \pi^+\pi^-$ search are estimated to be 44% and 41%, respectively. The contributions in many other modes become more than 50%, because background statistics of the atmospheric neutrino MC are poor. The uncertainties in all of the searches are summarized at Table I.

F. Results

In the absence of any significant nuleon decay signature, we interpret our results as lower limits of nucleon partial lifetime for each decay mode using the following method [31].

First, based on Bayes theorem, we calculate the nucleon decay probability, $P(\Gamma|n_i)$, as follows:

$$P(\Gamma|n_i) = A \int\int\int \frac{e^{-(\Gamma\lambda_i\epsilon_i+b_i)}(\Gamma\lambda_i\epsilon_i+b_i)^{n_i}}{n_i!} P(\Gamma)P(\lambda_i)P(\epsilon_i)P(b_i)d\lambda_i d\epsilon_i db_i. \tag{4}$$

Here a Poisson distribution is assumed for the nucleon decay probability; n_i is the number of candidate events in the i-th nucleon decay search; Γ is the total decay rate; λ_i is the corresponding detector exposure; ϵ_i is the detection efficiency including the meson branching ratio; and b_i is the expected background. In our search, λ_i is 3.05×10^{34} proton·year for proton decay and 2.44×10^{34} neutron·year for neutron decay. $P(\Gamma)$ is the decay rate probability density. We assume $P(\Gamma)$ as one for $\Gamma > 0$ and otherwise zero. The uncertainties of detector exposure ($P(\lambda_i)$), detection efficiency ($P(\epsilon_i)$) and background ($P(b_i)$) are expressed as follows:

$$P(\lambda_i) = \delta(\lambda_i - \lambda_{0,i}) \tag{5}$$

$$P(\epsilon_i) = e^{-(\epsilon_i - \epsilon_{0,i})^2/2\sigma_{\epsilon,i}^2} \ (0 \le \epsilon_i \le 1, \text{otherwise } 0) \tag{6}$$

$$P(b_i) = \frac{1}{b_i} \int_0^\infty \frac{e^{-b'}(b')^{n_{b,i}}}{n_{b,i}!} e^{-\frac{-(b_i C_i - b')^2}{2\sigma_{b,i}^2}} db' \\ (0 \le b_i, \text{otherwise } 0), \tag{7}$$

where $\lambda_{0,i}$ is the estimated exposure, $\epsilon_{0,i}$ is the estimated detection efficiency, $\sigma_{\epsilon,i}$ is the estimated uncertainty in the detection efficiency, $n_{b,i}$ is the number of background events, C_i is the MC oversampling factor, and $\sigma_{b,i}$ is the

uncertainty in the background. Because the uncertainty in the exposure is small, a delta function is assumed for $P(\lambda_i)$. The lower limit of the nucleon decay rate, Γ_{limit}, is calculated using Equation 8, where n is the number of searches for a decay mode. In our search, we calculate 90% confidence level (CL) limit, i.e., $CL = 0.9$ as follows:

$$CL = \frac{\int_{\Gamma=0}^{\Gamma_{limit}} \prod_{i=1}^{n} P(\Gamma|n_i)d\Gamma}{\int_{\Gamma=0}^{\infty} \prod_{i=1}^{n} P(\Gamma|n_i)d\Gamma}. \tag{8}$$

The lower limit of partial nucleon lifetime, τ/B, is now calculated by:

$$\tau/B = \frac{1}{\Gamma_{limit}} \sum_{i=1}^{n} [\epsilon_{0,i} \cdot \lambda_{0,i}]. \tag{9}$$

In the $p \to \bar{\nu}K^+$, prompt gamma-ray and $K^+ \to \pi^+\pi^0$ search, the lower limit of the nucleon partial lifetime is found to be 1.0×10^{33} years and 7.8×10^{32} years at 90% CL, respectively. Only for $p \to \bar{\nu}K^+$, mono-energetic muon search, we use a special method because it has a lot of background. We search for an excess in the signal region (B3) of the muon momentum distribution. After applying criteria (B1,B2,B7), the events are divided

into three momentum bins; p_μ are 200-215 MeV/c, 215-260 MeV/c and 260-305 MeV/c. The numbers of events in each momentum bin (n_1, n_2, n_3) are 76, 181, 185 events, respectively. The expected numbers of neutrino MC events in each momentum bin (b_1, b_2, b_3) are 78, 223, 182 events, respectively. The nucleon decay probabilities, $P(\Gamma|n_1, n_2, n_3)$, is then calculated using Equation 10:

$$P(\Gamma|n_1, n_2, n_3) = A \int\int\int \prod_{i=1}^{3} \frac{e^{-(\Gamma\lambda_i\epsilon_i + b_{shape,i}*b)}(\Gamma\lambda_i\epsilon_i + b_{shape,i}*b)^{n_i}}{n_i!} P(\Gamma)P(\lambda_i)P(\epsilon_i)P(b)P(b_{shape,i})d\lambda_i d\epsilon_i db db_{shape,i},$$

(10)

where $i = 1, 2, 3$, corresponds to 200-215 MeV/c, 215-260 MeV/c and 260-305 MeV/c, respectively; $P(b)$ is defined as one for $0 < b$ and otherwise zero; ϵ_1, ϵ_2, and ϵ_3 are estimated to be 0.25%, 34% and 1.3%, respectively. The background shape, $b_{shape,i}$, is b_i divided by b_2. The uncertainty function of the background shape $P(b_{shape,i})$ is defined to be a Gaussian function for $i = 1, 3$ and a delta function for $i = 2$. The uncertainties for $i = 1, 3$ are then estimated to be 7% and 8% from the MC model difference, respectively. From Equations 8 and 9 using $P(\Gamma|n_1, n_2, n_3)$ instead of $P(\Gamma|n_i)$, decay limit is calculated to be 6.4×10^{32} years at 90% CL. Using the three methods, the combined lower limit on the partial lifetime of proton via $p \to \bar{\nu}K^+$ is 2.3×10^{33} years at 90% CL.

In the $n \to \bar{\nu}K^0$ analysis, although we observe more events than the expected background in the $K_S^0 \to \pi^+\pi^-$ search, there is no excess in the $K_S^0 \to \pi^0\pi^0$ search. Therefore we also set a nucleon decay lifetime limit in this article. Combining two methods, we obtain the lifetime limit of 1.3×10^{32} years at 90% CL. In the $p \to \mu^+K^0$ and $p \to e^+K^0$ search, by combining three methods, the lifetime lower limits are set to be 1.3×10^{33} years and 1.0×10^{33} at 90% CL, respectively. The limits in all searches are summarized at Table I.

VII. CONCLUSION

We have searched for nucleon decay via $p \to \bar{\nu}K^+$, $n \to \bar{\nu}K^0$, $p \to \mu^+K^0$ and $p \to e^+K^0$ from an exposure of 92 kt·year. No significant excess above background is observed. The lower limits of the partial nucleon lifetime at 90% CL for each mode are 2.3×10^{33}, 1.3×10^{32}, 1.3×10^{33} and 1.0×10^{33} years, respectively (See Table I). From these results minimal SUSY SU(5) is fully excluded [9]. These results also give strong constraints on other SUSY GUT models [8, 11].

[1] J.C.Pati and A.Salam, Phys. Rev. Lett.**31**, 661 (1973).
[2] H.Georgi and S.L.Glashow, Phys. Rev. Lett. **32**, 438 (1974).
[3] C.McGrew *et al.*, Phys. Rev. **D59**, 052004 (1999).
[4] K.Hirata *et al.*, Phys. Lett. **B220**, 308 (1989).
[5] M.Shiozawa *et al.*, Phys. Rev. Lett. **81**, 3319 (1998).
[6] J.Wess and B.Zumino, Nucl. Phys. **B70**, 39 (1974).
[7] U.Amaldi *et al.*, Phys. Lett. **B260**, 447 (1991).
[8] N.Sakai and T.Yanagida, Nucl. Phys. **B197**, 533 (1982); S.Weinberg, Phys. Rev. **D26**, 287 (1982); J.Ellis *et al.*, Nucl. Phys. **B202**, 43. (1982); P.Nath *et al.*, Phys. Rev. **D32**, 2348 (1985); P.Nath *et al.*, Phys. Rev. **D38**, 1479 (1988); J.Hisano *et al.*, Nucl. Phys. **B402**, 46 (1993); T.Goto and T.Nihei, Phys. Rev. **D59**, 115009 (1999).
[9] H.Murayama and A.Pierce, Phys. Rev. **D65**, 055009 (2002).
[10] Y. Fukuda *et al.*, Phys. Rev. Lett. **81**, 1562 (1998).
[11] K.S.Babu, J.C.Pati and F.Wilczek, Phys. Lett. **B423**, 337 (1998); J.C.Pati hep-ph/0204240.
[12] G.Battistoni *et al.*, Phys. Lett. **B133**, 454 (1984); C.Berger *et al.*, Nucl. Phys. **B313**, 509 (1989); C.Berger *et al.*, Z. Phys. **C50**, 385 (1991); W.Allison *et al.*, Phys. Lett. **B427**, 217 (1998).
[13] D.Wall *et al.*, Phys. Rev. Lett. **D61**, 072004 (2000).

TABLE I: Summary of nucleon decay search. The numbers in the parentheses are the systematic uncertainties (%).

mode	method	efficiency (%)	background	candidate	lower limit ($\times 10^{32}$years)
$p \to \bar{\nu} K^+$	total				23
	prompt gamma-ray search	8.6 (20.)	0.7 (59.)	0	10.
	mono-energetic muon search	35.6 (2.5)	—	—	6.4
	$K^+ \to \pi^+ \pi^0$ search	6.0 (8.8)	0.6 (74.)	0	7.8
$n \to \bar{\nu} K^0$	total				1.3
	$K_S^0 \to \pi^0 \pi^0$	6.9 (16.)	19. (44.)	14	1.3
	$K_S^0 \to \pi^+ \pi^-$	5.5 (14.)	11. (41.)	20	0.69
$p \to \mu^+ K^0$	total				13
	$K_S^0 \to \pi^0 \pi^0$	5.4 (11.)	0.4 (78.)	0	7.0
	$K_S^0 \to \pi^+ \pi^-$ Method 1	7.0 (9.5)	3.2 (41.)	3	4.4
	$K_S^0 \to \pi^+ \pi^-$ Method 2	2.8 (12.)	0.3 (76.)	0	3.6
$p \to e^+ K^0$	total				10
	$K_S^0 \to \pi^0 \pi^0$	9.2 (5.8)	1.1 (62.)	1	8.4
	$K_S^0 \to \pi^+ \pi^-$ Method 1	7.9 (12.)	3.6 (50.)	5	3.5
	$K_S^0 \to \pi^+ \pi^-$ Method 2	1.3 (19.)	0.04 (146.)	0	1.6

[14] S. Fukuda *et al.*, Nucl. Inst. and Meth. **A501**, 418 (2003).
[15] K.Nakamura *et al.*, Nucl. Phys. **A268**, 381 (1976).
[16] T.Yamazaki and Y.Akaishi, Phys. Lett. **B433**, 1 (1999).
[17] H.Ejiri, Phys. Rev. **C48**, 1442 (1993).
[18] R.Woods and D.Saxon, Phys. Rev. **95**, 577 (1954).
[19] J.Hyslop *et al.*, Phys. Rev. **D46**, 961 (1992).
[20] R.Glasser *et al.*, Phys. Rev. **D15**, 1200 (1977).
[21] CERN Program Library W5013 (1994).
[22] M.Nakahata *et al.*, J. Phys. Soc. Jpn. **55**, 3786 (1986); A.S.Clough *et al.*, Nucl. Phys. **B76** 15 (1974).
[23] J.P.Albanese *et al.*, Nucl. Phys. **A350** 301 (1980); C.H.Q.Ingram *et al.*, Phys. Rev. **C27** 1578 (1983).
[24] T.A.Gabriel *et al.*, IEEE Trans. Nucl. Sci. **36**, 14 (1989).
[25] M.Honda *et al.*, Phys. Rev. **D52**, 4985 (1995); M.Honda *et al.*, Phys. Rev. **D64**, 053011 (2001).
[26] to be published.
[27] A.Bodek and U.K.Yang, hep-ex/0203009.
[28] D.Rein and L.M.Sehgal, Ann. of Phys. **133**, 79 (1981); D.Rein, Z. Phys. **C35**, 43 (1987).
[29] Y.Hayato *et al.*, Phys. Rev. Lett. **83**, 1529 (1999).
[30] C.Carone *et al.* Phys. Rev. **D53** 6282 (1996).
[31] Particle Data Group, Review of Particle Physics, Section: Errors and confidence intervals – Bounded physical region, June 1996: R.M. Barnett *et al.*, Phys. Rev. **D54**, 375 (1996).